

# Plasmonic optical properties of a single gold nano-rod

Hung Ji Huang<sup>1,2</sup>, Chin Ping Yu<sup>2,3</sup>, Hung Chun Chang<sup>3</sup>, Kuo Pin Chiu<sup>1,2</sup>, Hao Ming Chen<sup>4</sup>, Ru Shi Liu<sup>4</sup>, and Din Ping Tsai<sup>1,2,5,6\*</sup>

<sup>1</sup>Department of Physics, National Taiwan University, Taipei 10617, Taiwan

<sup>2</sup>Center of Nanostorage Research, National Taiwan University, Taipei 10617 Taiwan

<sup>3</sup>Graduate Institute of Electro-Optical Engineering, National Taiwan University, Taipei, Taiwan 10617

<sup>4</sup>Department of Chemistry, National Taiwan University, Taipei, Taiwan 10617

<sup>5</sup>Institute of Electro-optical Science and Technology, National Taiwan Normal University, Taipei 116, Taiwan

<sup>6</sup>Research Center for Applied Sciences, Academia Sinica, Taipei 115, Taiwan

[dptsai@phys.ntu.edu.tw](mailto:dptsai@phys.ntu.edu.tw)

**Abstract:** Polarization-contrast microscopy coupled with an atomic force microscope is utilized to attain far-field optical images of the multipolar surface plasmon resonance (SPR) modes of single gold nano-rod. Modulated standing modes resulted from the interference of longitudinal SPR modes and incident light are observed and studied. By counting the average distance of adjacent beats on this single gold nano-rod, the wave vector of longitudinal SPR modes can be obtained. We found a linear relationship between the wave vectors of the incident light and the induced SPR modes. Experimental results demonstrate a feasible way on acquiring plasmonic optical properties from an individual single gold nano-rod.

©2007 Optical Society of America

**OCIS codes:** (240.6680) Surface plasmons; (260.3910) Metals, optics of; (160.4760) Optical properties.

---

## References and links

1. A. Christ, T. Zentgraf, J. Kuhl, S. G. Tikhodeev, N. A. Gippius, and H. Giessen, "Optical properties of planar metallic photonic crystal structures: Experiment and theory," *Phys. Rev. B* **70**, 125113 (2004).
2. S. I. Bozhevolnyi, J. Erland, K. Leosson, P. M. W. Skovgaard, and J. M. Hvam, "Waveguiding in surface plasmon polariton band gap structures," *Phys. Rev. Lett.* **86**, 3008 (2001).
3. F. I. Baida, D. van Labeke, Y. Pagani, B. Guizal, and M. al Naboulsi, "Waveguiding through a two-dimensional metallic photonic crystal," *J. Microsc.* **213**, 144–148 (2004).
4. M. Quinten, A. Leitner, J. R. Krenn, and F. R. Aussenegg, "Electromagnetic energy transport via linear chains of silver nanoparticles," *Opt. Lett.* **23**, 1331–1333 (1998).
5. M. L. Brongersma, J. W. Hartman, and H. A. Atwater, "Electromagnetic energy transfer and switching in nanoparticle chain arrays below the diffraction limit," *Phys. Rev. B* **62**, R16356–R16359 (2000).
6. T. W. Ebbesen, H. J. Lezec, H. F. Ghaemi, T. Thio, and P. A. Wolff, "Extraordinary optical transmission through sub-wavelength hole arrays," *Nature (London)* **391**, 667–669 (1998).
7. W. C. Tan, T. W. Preist, R. J. Sambles, and N. P. Wanstall, "Flat surface-plasmon-polariton bands and resonant optical absorption on short-pitch metal gratings," *Phys. Rev. B* **59**, 12661–12666 (1999).
8. L. Martín-Moreno, F. J. García-Vidal, H. J. Lezec, K. M. Pellerin, T. Thio, J. B. Pendry, and T. W. Ebbesen, "Theory of extraordinary optical transmission through subwavelength hole arrays," *Phys. Rev. Lett.* **86**, 1114–1117 (2001).
9. D. P. Tsai, C. W. Yang, W. C. Lin, F. H. Ho, H. J. Huang, M. Y. Chen, T. F. Tseng, C. H. Lee, and C. J. Yeh "Dynamic aperture of near-field super resolution structures," *Jpn. J. Appl. Phys.* **39**, 982–983 (2000).
10. W. C. Liu and D. P. Tsai, "Optical tunneling effect of surface plasmon polaritons and localized surface plasmon resonance," *Phys. Rev. B* **65**, 155423 (2001).
11. M. Moskovits, "Surface-enhanced spectroscopy," *Rev. Mod. Phys.* **57**, 783–826 (1985).
12. S. Nie and S. R. Emory, "Probing single molecules and single nanoparticles by surface-enhanced Raman Scattering," *Science* **275**, 1102–1106 (1997).
13. H. Xu, E. J. Bjerneld, M. Kall, and L. Borjesson, "Spectroscopy of single hemoglobin molecules by surface enhanced Raman scattering," *Phys. Rev. Lett.* **83**, 4357 (1999).
14. D. P. Tsai and W. C. Lin, "Probing the near fields of the super-resolution near-field optical structure," *Appl. Phys. Lett.*, **77**, 1413–1415 (2000).

15. F. H. Ho, W. Y. Lin, H. H. Chang, Y. H. Lin, W. C. Liu, and D. P. Tsai, "Nonlinear optical absorption in the AgO<sub>x</sub>-type super-resolution near-field structure," *Jpn. J. Appl. Phys.* **40**, 4101–4102 (2001).
16. T. C. Chu, W. C. Liu, and D. P. Tsai, "Enhanced resolution induced by random silver nanoparticles in near-field optical disks," *Opt. Commun.* **246**, 561–567 (2005).
17. T. Klar, M. Perner, S. Grosse, G. von Plessen, W. Spirkl, and J. Feldmann, "Surface-plasmon resonances in single metallic nanoparticles," *Phys. Rev. Lett.* **80**, 4249–4252 (1999).
18. K. Imura, T. Nagahara, and H. Okamoto, "Characteristic near-field spectra of single gold nanoparticles," *Chem. Phys. Lett.* **400**, 500–505 (2004).
19. K. Imura, T. Nagahara, and H. Okamoto, "Near-field two-photon-induced photoluminescence from single gold nanorods and imaging of plasmon modes," *J. Phys. Chem. B* **109**, 13214–13220 (2005).
20. G. Laurent, N. Féridj, J. Aubard, and G. Lévi, "Evidence of multipolar excitations in surface enhanced Raman scattering," *Phys. Rev. B* **71**, 45430 (2005).
21. E. K. Payne, K. L. Shuford, S. Park, G. C. Schatz, and C. A. Mirkin, "Multipole plasmon resonances in gold nanorods," *J. Phys. Chem. B* **110**, 2150–2154 (2006).
22. P. Muhschlegel, H. J. Eisler, O. J. F. Martin, B. Hecht, and D. W. Pohl, "Resonant optical antennas," *Science* **308**, 1607 (2005).
23. C. Sonnichsen and A. P. Alivisatos, "Gold nanorods as novel nonbleaching plasmon-based orientation sensors for polarized single-particle microscopy," *Nano Lett.* **5**, 301–304 (2005).
24. A. Ono, J. Kato, and S. Kawata, "Subwavelength optical imaging through a metallic nanorod array," *Phys. Rev. Lett.* **95**, 267407 (2005).
25. J. C. Weeber, A. Dereux, C. Girard, J. R. Krenn, and J. P. Goudonnet, "Plasmon polaritons of metallic nanowires for controlling submicron propagation of light," *Phys. Rev. B* **60**, 9061 (1999).
26. H. Ditlbacher, A. Hohenau, D. Wagner, U. Kreibig, M. Rogers, F. Hofer, F. R. Aussenegg, and J. R. Krenn, "Silver nanowires as surface plasmon resonators," *Phys. Rev. Lett.* **95**, 257403 (2005).
27. J. Aizpurua, G. W. Bryant, L. J. Richter, and F. J. García de Abajo, B. K. Kelley, and T. Mallouk, "Optical properties of coupled metallic nanorods for field-enhanced spectroscopy," *Phys. Rev. B* **71**, 235420 (2005).
28. G. Schider, J. R. Krenn, A. Hohenau, H. Ditlbacher, A. Leitner, and F. R. Aussenegg, "Plasmon dispersion relation of Au and Ag nanowires," *Phys. Rev. B* **68**, 155427 (2003).
29. K. Imura, T. Nagahara, and H. Okamoto, "Near-field optical imaging of plasmon modes in gold nanorods," *J. Chem. Phys.* **122**, 154701 (2005).
30. N. Féridj, G. Laurent, J. Grand, J. Aubard, G. Lévi, A. Hohenau, F. R. Aussenegg, and J. R. Krenn, "Far-field Raman Imaging of short-wavelength particle plasmons on gold nanorods," *Plasmonics* **1**, 35–39 (2006).
31. N. Taub, O. Krichevski, and G. Markovich, "Growth of gold nanorods on surfaces," *J. Phys. Chem. B* **107**, 11579–11582 (2003).
32. H. M. Chen, H. C. Peng, R. S. Liu, K. Asakura, C. L. Lee, J. F. Lee and S. F. Fu, "Controlling the Length and Shape of Gold Nanorods," *J. Phys. Chem. B* **109**, 19553 (2005).
33. J. Seidel, F. I. Baida, L. Bischoff, B. Guizal, S. Grafström, D. van Labeke, and L. M. Eng, "Coupling between surface plasmon modes on metal films," *Phys. Rev. B* **69**, 121405 (2004).

## 1. Introduction

In recent years, there is a growing research interest toward the interaction of light with nanosized metallic structures for the property of driving oscillations of collective free electrons on the surface of the metal under proper conditions, called surface plasmons (SPs). It is well known that SPs contribute to various novel applications in nano-optics and the localized field enhancement for near-field measurements. Waveguides based on SPs can provide strong guidance of light via periodic metallic structures [1-3] or metallic particle chains [4-5]. Even for sharp bending, strong light confinements can be achieved [2, 3]. By introducing some apertures or grooves in metallic films to induce localized SPs, the transmission of light can be highly promoted [6-10]. The SPs also play an important role in near-field optical measurements. The enhancement of light by metallic nano-structure leads to useful applications such as the surface-enhanced Raman scattering (SERS) [11-13] and near-field optical disks [14-16].

Among these metallic nano-structures, metallic nano-rods attract more attentions for their geometric anisotropy in the cross section and length. In particular, gold and silver nano-rods received specific research efforts for their surface plasmon resonances (SPRs) falling in the visible region or the near-infrared regime. Except the similar transverse SPRs observed in spherical metallic particles [17, 18], metallic nano-rods exhibit multipolar longitudinal SPRs [19-21]. By varying the length, the cross section, and the surrounding medium of nano-rods,

the resonant wavelength of the SPRs can be efficiently tuned leading to the applications of antennas [22], orientation detectors [23], and nano-imaging [24]. The metallic nano-rods also provide another efficient way to guide light in nano-optical system [24-26]. In addition, the enhancement of light in the middle gaps of coupled nano-rod structures can also be utilized in SERS [27].

Many research efforts are devoted to obtain the optical properties of gold nano-rods. Schider *et al.* used optical extinction spectroscopy of silver and gold nano-rod arrays fabricated by electron-beam lithography (EBL) to determine the wave vectors of excited SPR modes [28]. These metallic nano-rods separated in 1  $\mu\text{m}$  and the resulted dispersion curves are similar to those of metallic thin films. Imura *et al.* utilized an apertured-type scanning near-field optical microscope (SNOM) to obtain the transmission spectrum of individual gold nano-rods fabricated by seed-mediated method [29]. The resonant wavelengths of SPRs and dispersion relation of gold nano-rods with fixed diameter and variant rod lengths were successfully obtained. However, the scanning probe in SNOM might cause some interactions with the metallic nano-rods and have some influence on the dispersion characteristics. To avoid possible interferences of the probe in near-field measurement, the far-field Raman scattering of methylene blue absorbed on the samples was adopted to image the gold nano-rod arrays made by EBL [30]. As a result of the interference of the longitudinal SPR modes and incident light, modulated field distribution along the nano-rods was observed.

Since gold nano-rods can function as fundamental building blocks in plasmonic integrated optics, it is crucial to know their individual optical properties, especially the relationship between the incident light and the induced SPR modes on each single nano-rod. In this paper, to avoid the complexity of the near-field systems and the influence caused by the probe, we use simple polarization-contrast microscopy to attain far-field images of a single gold nano-rod fabricated by chemical method. In particular, we will find out the wave vectors of the induced longitudinal SPR modes from the same gold nano-rod to obtain its individual optical properties.

## 2. Sample preparation and experimental setup

In our experiment, Au nano-rods were prepared with the hexadecyltrimethylammonium bromide (CTAB) soft template method based on the typical chemical reduction process proposed by Taub *et al.* and Chen *et al.* [31, 32]. The process can be described as the following four steps:

1. A seed solution was generated by adding sodium borohydride ( $\text{NaBH}_4$ ) into aqueous solution containing a mixture of gold tetrachloride ( $\text{HAuCl}_4$ ) and trisodium citrate. The average size of the deoxidized Au seeds is smaller than 4 nm.
2. The Borosilicate Crown (BK-7) cover glass slip was first steeped into the 3-aminopropyl-trimethoxy-silane (APTMS) solution. It was then cleaned by deionized water and heated to strengthen the bonding of Si-O-Si of the APTMS adhered on the cover glass slip. When the cover glass slip was soaked into the seed solution, the Au seeds were fixed to the top of the cover glass slip.
3. The growth solution was a CTAB solution containing 0.25 mM  $\text{HAuCl}_4$  and 1.5% acetone and 2% cyclohexane. The color of the growth solution was disappeared after ascorbic acid was added.
4. After putting the cover glass slip into the growth solution for 20 minutes in room temperature, the growth of Au nano-rods was terminated. The cover glass slip was then steeped and cleaned by deionized water for several times to remove the CATB, and Au nano-rods were obtained on the cover glass slip.

Following the steps described above, gold nano-rods with high aspect ratio from 12 to 16 can be attained. Figure 1(a) shows the AFM image of a single gold nano-rod with the diameter around 125 nm. The length of the nano-rod is 1.45  $\mu\text{m}$ , and the corresponding aspect ratio is around 12. One can clearly observe the shape of the nano-rod from Fig. 1(a). With the P-polarized (also parallel to the nano-rod) white light as the incident source, the far-field scattering image of this gold nano-rod is shown in Fig. 1(b). The observed gold nano-rod is

quite far away from other nano-particles to avoid possible interferences. Image of Fig. 1(b) shows several dark fringes along the gold nano-rod, which are the occurrences of multipolar SPR modes [30, 33].

Figure 1(c) is the schematic of experimental setup for the far-field optical observation. An inverted microscope system (IX-70; Olympus Inc.) equipped with a high numerical aperture (NA) objective (PlanApo, oil 100 $\times$ , NA from 0.5 to 1.35, Olympus Inc.) is used for optical imaging of the single gold nano-rod. The incident light is reflected by a movable rotation mirror on an adjustable steel rod with incident angle controlled to precision of 0.2 $^\circ$ . A polarizer of extinction ratio of 1000:1 is utilized to control the polarization of the incident light. The transmitted light after interacting with the single gold nano-rod is collected by an objective of 1.35 NA. A cross polarized analyzer (extinction ratio 1000:1) is behind the objective to filter out the incident light. We can then acquire the microscopic images by a TE-cooled charge-coupled device (CCD) camera or perform the spectra measurement by the spectrum meter. Figure 1(d) is the photograph of our home-made translation stage containing an atomic force microscope (AFM) (ND-MDT Inc. Smena-A) on the inverted optical microscope shown in Fig. 1(c). The topographic measurements and optical observations of the samples can be studied simultaneously. In addition, this polarization-contrast microscopy can efficiently reduce the optical background and provide a simple, inexpensive, and easily realized way to observe the metallic nano-particles such as gold nano-rods.

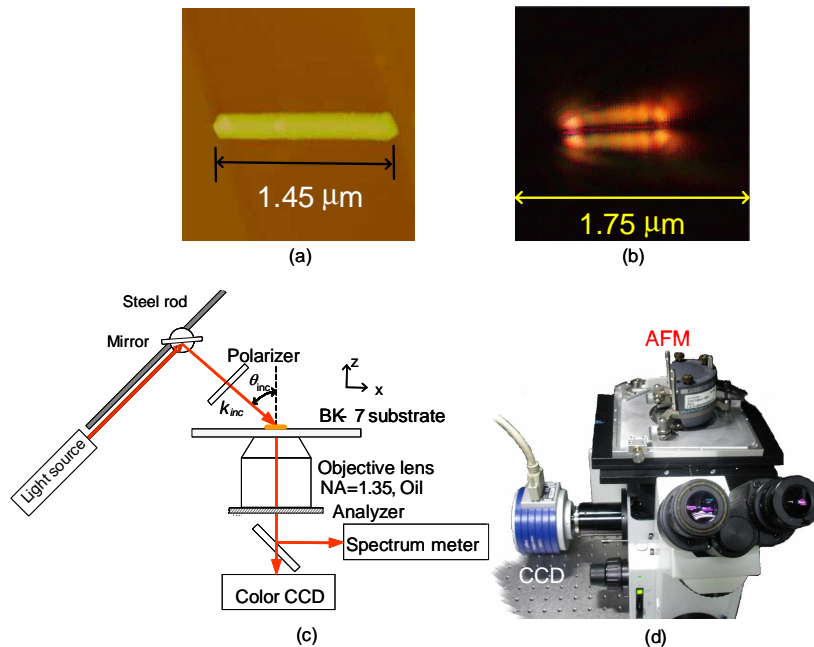


Fig. 1. (a) AFM image of a single gold nano-rod, and (b) a far-field image of the single gold nano-rod shown in (a) simultaneously. (c) Schematic and (d) photograph of the experimental setup.

### 3. Result and discussion

Figure 2 is the scattering spectrum of the single gold nano-rod shown in Figs. 1(a) and 1(b). After the P-polarized incident white light interacting with the gold nano-rod, the scattered light is collected by the objective and then passes through an analyzer. The incident angle  $\theta_{inc}$  is 51 $^\circ$  and the analyzer is placed perpendicularly to the polarized incident light to filter out the

background light. The spectrum in Fig. 2 is an extracted spectrum which has removed the luminescence caused by the substrate. In previous studies, it is found that gold nano-rods with larger aspect ratio have more induced longitudinal SPR modes [20, 21], and higher order longitudinal SPR modes will be appeared in the visible range, while lower ones are shifted towards infrared as we increase the nano-rod length [20, 28]. Thus, we can observe several peaks in the scattering spectrum in the visible region as shown in Fig. 2. However, the fundamental dipolar mode falls in longer wavelength region for the long axis of the nano-rod and can not be seen in this spectrum. Results showed background intensity of total scattered light is relatively large compared to that from the induced longitudinal SPR modes.

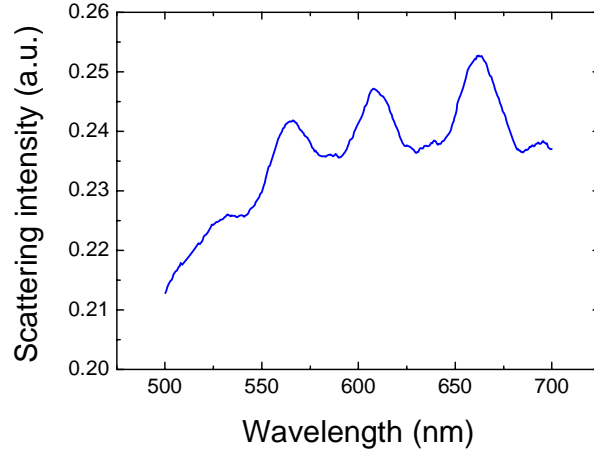


Fig. 2. Scattering spectrum of single gold nano-rod by using P-polarized incident white light with  $51^\circ$  incident angle.

To have a more clear insight of the appearance of the beats on the gold nano-rod, we consider a P-polarized incident light illuminated on a single gold nano-rod with an incident angle  $\theta_{inc}$  as shown in Fig. 3. The wave vector of the incident light can be divided into the parallel and perpendicular parts with respect to the nano-rod axis. The parallel part  $k_x$  can be expressed as

$$k_x = k_{inc} \cdot \sin \theta_{inc} = \frac{2\pi \sin \theta_{inc}}{\lambda_{inc}}, \quad (1)$$

where  $k_{inc}$  and  $\lambda_{inc}$  are the wave vector and wavelength of the incident light, respectively. As the incident light interacts with the nano-rod, the  $z$ -polarized electrical field will collect free electrons to the surface of the metallic nano-rod. Meanwhile, the  $x$ -polarized electrical field will drive these collective electrons to oscillate along the long axis of the nano-rod resulting in the longitudinal SPR mode with wave vector being  $k_{SPR}$ . In fact, the value of  $k_{SPR}$  is larger than  $k_x$  and even  $k_{inc}$ . To induce the  $k_{SPR}$  in the gold nano-rod, the limited geometrical structure and dramatically-terminated interface at the end of nano-rod contribute to the coupling of  $k_x$  to  $k_{SPR}$ , so called light-SPR transformation as indicated in Fig. 3.

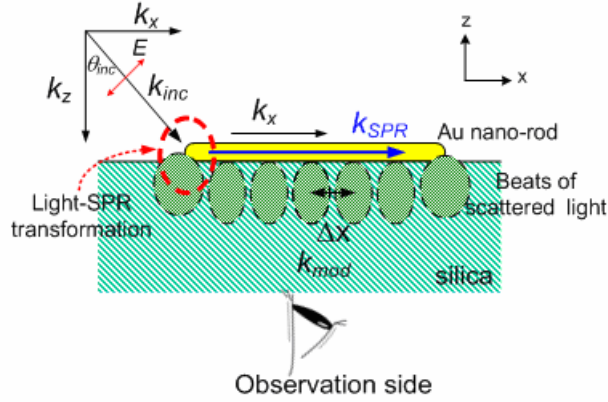


Fig. 3 Illustration of the relationship of the induced longitudinal SPR mode and the incident light.

The induced longitudinal SPR mode then propagates along the nano-rod axis and interferes with the existing parallel part of the incident light [30]. The interference of the two waves on the nano-rod results in the standing modulated mode with several “beats” (corresponding to maximum or minimum field intensities) along the gold nano-rod as shown in Fig. 1(b). As a result of the interference of two waves propagating in the same direction, the wave vector of the modulated modes can be expressed as

$$k_{\text{mod}} = \frac{k_{\text{SPR}} - k_x}{2} \quad (2)$$

[30, 32]. From the spacing of two adjacent beats observed in the far-field image of a single nano-rod, one can obtain the wavelength of the longitudinal SPR mode by

$$\lambda_{\text{SPR}} = 1 / \left( \frac{1}{\Delta x} + \frac{\sin \theta_{\text{inc}}}{\lambda_{\text{inc}}} \right), \quad (3)$$

where  $\Delta x = \pi / k_{\text{mod}}$ . Using variant  $\lambda_{\text{inc}}$  and  $\theta_{\text{inc}}$  (corresponding to variant  $k_x$ ), we can have the wavelengths of induced longitudinal SPR modes to construct the relationship between  $k_x$  and  $k_{\text{SPR}}$  as the light-SPR transformation on the gold nano-rod.

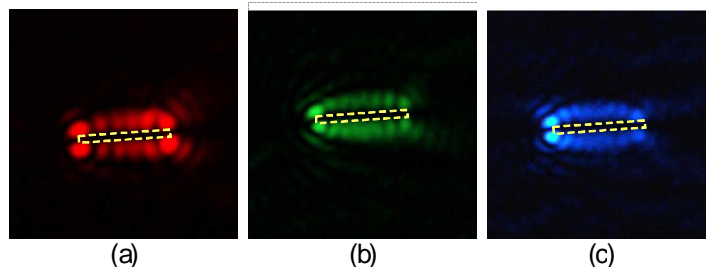


Fig. 4. Far-field images of SPR modes of the same single gold nano-rod for various incident laser light at (a) red (658 nm), (b) green (532 nm), and (c) blue (488 nm), respectively.

Instead of white light source, P-polarized red (658 nm), green (532 nm), and blue (488 nm) laser light are used as the incident light source, respectively. The images for various light sources with the analyzer in y-direction are shown in Figs. 4(a), (b), and (c), respectively. The dashed line represents the location of the measured single gold nano-rod. The modulated standing modes for the three wavelengths can be clearly seen, respectively. We found the

number of the light beats increases with the decrease of the incident wavelength. This is due to shorter incident wavelengths will induce higher order longitudinal SPR modes resulting in more light beats appeared on the gold nano-rod optical image. In addition, one can observe that light beats at both ends of the gold nano-rod have extended shapes as a result of change of light-SPR transformation and more radiations occurred at both ends of the nano-rod. These extending beats are not exactly located at the ends of the nano-rod as indicated in Fig. 3, and are demonstrated in these far-field scattering images shown in Fig. 4. Thus, using the total number of beats and rod-length to calculate the average beat-distance might result in possible errors. To obtain more accurate values of  $k_{SPR}$  for the induced SPR modes, only the beats in the central part of the nano-rod are taken into account on the measurements of  $\Delta x$ .

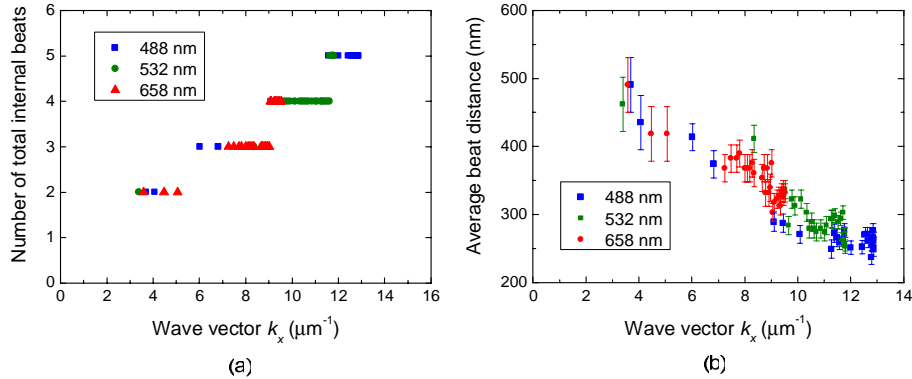


Fig. 5. (a) The observed numbers of beats (exclude beats at both ends of nano-rod) along a single gold nano-rod for various values of the parallel incident wave vector  $k_x$ . (b) Observed averaged beat distance ( $\Delta x$ ) for various wave vectors  $k_x$ . The square (blue), circular (green), and triangular (red) dots are the results of various incident laser wavelength of 488 nm, 532 nm, and 658 nm, respectively.

Based on results of three P-polarized laser light sources with various incident angles,  $\theta_{inc}$ , Fig. 5(a) shows the observed numbers of beats (exclude beats at both ends of nano-rod) for various values of the parallel incident wave vector  $k_x$ . We found step-like curve in Fig. 5(a) for the inducement of various longitudinal SPR modes. As we increase the value of  $k_x$ , higher-order SPR modes possessing larger  $k_{SPR}$ , and more light beats are induced. After interfering with incident light, more light beats on the gold nano-rod can be observed in far-field images. With the assistance of high spatial resolution AFM and clear polarization-contrast optical images, we found the average beat distance between two adjacent beats (exclude beats at both ends of nano-rod) and plotted in Fig. 5(b) for variant incident wave vector  $k_x$ . Again, the average beat distance increases with the decrease of  $k_x$  for the inducement of lower-order SPR modes.

From the values of  $k_{mod}$  and the corresponding incident wave vectors  $k_x$ , the  $k_{SPR}$  for the longitudinal SPR modes on the gold nano-rod can be deduced according to Eq. (3). The measured light-SPR transformation relationship of this gold nano-rod can then be obtained as shown in Fig. 6. The sharply-terminated surface of the gold nano-rod provides an effective coupling to excite longitudinal SPR modes as observed in our experimental results. The square, circular, and triangular dots are the results of various incident laser lights for the same single gold nano-rod. One can see that these dots form a linear-like relationship in Fig. 6. We have performed a linear fit in Fig. 6 and the value of  $k_{SPR} / k_x$  is around 2.3. The speed of plasmonic wave on this single gold nano-rod is 2.3 times slower than that of incident light. However, as the incident  $k_x$  increase (approaching the short wavelength region), undisguised higher-order longitudinal SPR modes and transverse SPR mode may be induced and results in the flatten shape at the end of the curve of Fig. 6.

Using the polarization-contrast microscopy, it is easy to have the far-field images of each single gold nano-rod along with their wave vectors of the induced different SPR modes. These measured results are from the same gold nano-rod and contribute to characterize the individual light-SPR transformation of the single gold nano-rod. The meta-materials based on these metallic nano-particles and nano-rods attract lots of attentions lately. It is crucial to have a good understanding of the plasmonic optical properties of each individual metallic nano-particles and nano-rods with various incident lights. Our experiments demonstrate a simple, inexpensive, and feasible way to attain the plasmonic optical properties of such an individual single building block of advanced future plasmonic devices. Moreover, these obtained unique properties of each nano-particle and nano-rod can readily assist the study of nano optics, and the development of novel applications of plasmonic nanophotonics.

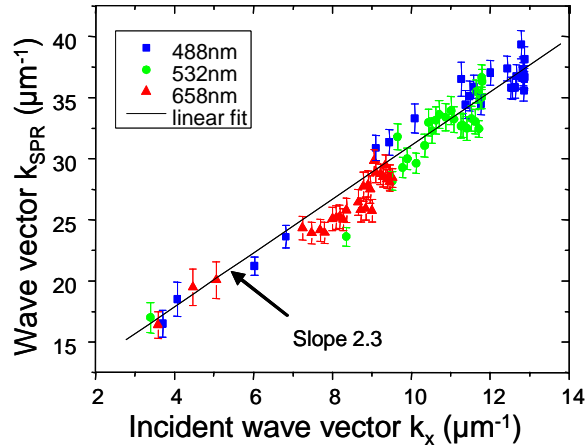


Fig. 6. Optical relationship of the induced SPR modes versus the parallel incident wave vectors  $k_x$ . The square (blue), circular (green), and triangular (red) dots are the results of various incident laser wavelength of 488 nm, 532 nm, and 658 nm, respectively.

## 7. Conclusion

We demonstrate far-field images of longitudinal SPR modes of single gold nano-rod by the polarization-contrast microscopy. The induced SPR modes interfering with incident light results in the modulated standing-wave-like modes along the gold nano-rod. Results show clear light beats along the gold nano-rod in the far-field optical images. The wave vectors of SPR modes can then be deduced to construct the light-SPR transformation relationship between the incident light and the induced SPR modes. Instead of using gold nano-rods with various sizes, we utilize the same single gold nano-rod for the measurements to obtain its individual optical properties. Our experiments can be very useful for acquiring the individual optical properties of gold nano-rods or similar fundamental building blocks in complicated nano-devices of plasmonic nanophotonics.

## Acknowledgments

The authors are grateful for the research support from the National Science Council of Taiwan, R.O.C. under project number NSC 95-2112-M-002-036-MY2 and NSC 95-2623-7-002-015, and the Ministry of Economic Affairs, R.O.C. under project number 95-EC-17-A-08-S1-0006. D. P. Tsai thanks the support from Center for Nano Science and Technology, National Taiwan University. Correspondence should be addressed to Din Ping Tsai by [dptsai@phys.ntu.edu.tw](mailto:dptsai@phys.ntu.edu.tw).